Atomic Force Microscopy and Light Scattering of Small Unilamellar Actin-Containing Liposomes

Andre F. Palmer, Philip Wingert, and Jonathan Nickels
Department of Chemical and Biomolecular Engineering, Center for Molecularly Engineered Materials, University of Notre Dame, Notre Dame, Indiana

ABSTRACT Three-dimensional networks of filamentous actin (F-actin) encapsulated inside phosphatidylcholine liposomes are currently being used in an effort to model the cytoskeleton and plasma membrane of eukaryotic cells. In this article, unilamellar lipid vesicles consisting of egg yolk-derived phosphatidylcholine encapsulating monomeric actin (G-actin) were made via extrusion in low ionic strength buffer (G-buffer). Vesicle shape and structure in these dispersions was studied using a combination of fluid-tapping atomic force microscopy, and multiangle static light scattering. After subjecting the liposome dispersion to high ionic strength polymerization buffer (F-buffer) containing K^+ ions, atomic force microscopy imaging and light scattering of these liposomes indicated the formation of specialized structures, including an overall liposome structure transformation from spherical to torus, disk-shaped geometries and tubular assemblies. Several atomic force microscopy control measurements were made to ascertain that the specialized structures formed were not due to free G-actin and F-actin self-assembling on the sample surface, plain liposomes exposed to G- and F-buffer, or liposomes encapsulating G-actin. Liposomes encapsulating G-actin assumed mostly thin disk shapes and some large irregularly shaped aggregates. In contrast, liposomes encapsulating polymerized actin assumed mostly torus or disk shapes along with some high aspect ratio tubular structures.

INTRODUCTION

Liposomes have been widely used to study many aspects of eukaryotic cell function such as aggregation, fusion, and selective permeability (Hotani et al., 1999; Jass et al., 2000; Teschke, 2002; Stauch et al., 2002). However, plain liposomes are not suitable for studying the interaction between lipid bilayers and cytoskeletal networks due to their inability to respond to shear stress like normal cells. For example, changes readily occur in the shapes of plain unilamellar liposomes when sheared, often leading to pronounced deformations and/or complete destruction (Reviakine and Brisson, 2000).

A more detailed model of the eukaryotic cell would include a cytoskeletal matrix that is surrounded by a lipid membrane. This could be accomplished by encapsulating, either singly or in combination, semiflexible filaments (e.g., actin), intermediate filaments (e.g., keratin), or rigid rod filaments (e.g., microtubules) inside the aqueous core of a liposome. These artificial structures are significant in that they provide researchers with a minimalist model of the cell, which mimics both the cell membrane and the underlying cytoskeletal matrix. The use of liposomes encapsulating cytoskeletal filaments makes it possible to study, in a reconstituted system, remodeling of the lipid membrane and actin cytoskeleton during important cellular processes such as cell motility, cytokinesis, pinocytosis, and phagocytosis (Lodish et al., 1999; Stauch et al., 2002).

Submitted January 27, 2003, and accepted for publication April 3, 2003.

Address reprint requests to Andre F. Palmer, Dept. of Chemical and Biomolecular Engineering, Center for Molecularly Engineered Materials, University of Notre Dame, Notre Dame, IN 46556. Tel.: 574-631-4778; Fax: 574-631-4776; E-mail: apalmer@nd.edu.

0006-3495/03/08/1233/15 $2.00

Hotani and Miyamoto (1990) were one of the first groups to polymerize the cytoskeletal monomeric protein tubulin inside the aqueous core of giant liposomes. The unpolymerized tubulin encapsulated within the liposomes assumed a spherical shape. However, when the encapsulated tubulin was polymerized into rod-shaped microtubules, the initially spherical liposomes transformed first into a rugby-ball geometry, then into a bipolar geometry.

More realistic cellular models have since been created by substituting the cytoskeletal polymer actin instead of tubulin inside the liposome aqueous core. Two experimental methods of preparing these assemblies are commonly used.

In the first method, a dried lipid film is hydrated with G-actin in aqueous solution at 0°C (Miyata and Hotani, 1992). Giant liposomes encapsulating G-actin spontaneously formed under these conditions. However, this method yielded low numbers of giant liposomes. To polymerize the encapsulated actin within the liposome, two techniques are commonly employed. The first method induces G-actin polymerization into filamentous actin (F-actin) by increasing the temperature of G-actin liposome dispersions (Miyata and Hotani, 1992). The initially spherically shaped liposomes deformed into both dumbbell or disk geometries. The second method creates transient pores in the liposome membrane by electroporation (Miyata et al., 1999). This permits KCl in the bulk solution to diffuse into the aqueous core of the liposome through the transient pores, which polymerizes the G-actin. In this case thin protrusive invaginations consisting of actin filaments encased in a lipid bilayer extended from the surface of the initially spherical liposome surface.

In the second method of preparing actin-containing liposomes, the dried lipid film is hydrated with G-actin in aqueous buffer in the presence of an AC field (Häckl at al.,

1998). This method forms a monodisperse population of spherical giant actin-containing liposomes in high yield. Polymerization was induced by adding Mg^{2+} ions into the bulk solution, which diffused into the liposome through Mg^{2+} ion channels, thus polymerizing the G-actin. The resultant giant actin-liposome retains its spherical shape. However, a thin actin shell or cortex develops around the inside leaflet of the giant liposome. The authors studied the fluctuation of the giant actin-containing liposome bilayer to measure its bending modulus. They inferred from this measurement that the actin shell was uncoupled to the liposome lipid bilayer.

Boulbitch et al. (2000) also studied giant liposomes with an underlying actin cortex and showed that the presence of this cortex triggered local shape instabilities in the associated lipid bilayer membrane, forming blisters when the temperature was slightly increased. In an extension of the previously mentioned studies, Helfer et al. (2001) studied a self-assembled network of actin filaments attached to the outer surface of giant liposomes and found that the presence of this network strongly modifies the membrane dynamics from that seen with an uncoated lipid bilayer. In all G-actin-containing liposome production schemes, the resulting giant liposomes assumed spherical shapes.

Recent developments in atomic force microscopy (AFM) have led to direct in situ observation of many biological materials including phospholipid bilayer membranes (Shao and Yang, 1995; Balashev et al., 2001), membrane proteins in lipid bilayers (Puu et al., 2000), and liposomes (Egawa and Furusawa, 1999; Jass et al., 2000; Thomson et al., 2000). To our knowledge, no one has used AFM and multiangle static light-scattering (MASLS) to determine the structure of liposomes encapsulating the cytoskeletal polymer actin. Furthermore, no one has studied encapsulated actin in small, unilamellar vesicles <0.5 μm in diameter; thus, our study provides a model system to study cytoskeletal organization in liposomes much smaller than those previously studied.

MATERIALS AND METHODS

Chemicals

L-α-Phosphatidylcholine (PC) derived from egg-yolk tissue with >99% purity was obtained from Avanti Polar Lipids (Alabaster, AL) and stored in chloroform stock solutions at -20°C. Monomer actin, G-buffer (5 mM tris-HCl, pH 8.0, 0.2 mM $CaCl_2$, and 0.2 mM ATP), and F-buffer (50 mM KCl, 2 mM $MgCl_2$, and 1mM ATP) were obtained from Cytoskeleton (Denver, CO). K^+ ionophore was obtained from Fluka (Buchs, Switzerland). All water was taken from a Barnstead E-Pure (Barnstead/Thermolyne, Dubuque, IA) ultra-pure water system with a resistivity of 18.1 MΩ-cm and filtered with 0.02 μm inorganic membrane filters obtained from Whatman (Maidstone, England).

G-buffer was used for all AFM imaging and MASLS studies of G-actin, plain liposomes, and liposomes encapsulating G-actin. F-buffer was used for all studies of polymerized G-actin, plain liposomes, and liposomes encapsulating G-actin under polymerizing conditions.

Atomic force microscopy

All imaging was performed using a Digital Instruments (Santa Barbara, CA) Nanoscope IV Multimode AFM system fitted with a vertical E or J scanner (15 $\times$ 15 μm scan size, and 3.64 μm vertical range or 125 $\times$ 125 μm scan size, and 5.65 μm vertical range, respectively) and a tapping mode fluid cell. All imaging was done in fluid-tapping mode using a modified O-ring method. Cantilevers with 100 μm, narrowed-leg, oxide-sharpened Si_3N_4 tips with a nominal spring constant of $\sim$0.32 N/m were used. The cantilevers were acoustically excited indirectly both through the cell and the liquid at frequencies between 9 and 10 kHz, which is just below their resonant frequency in water. Scan rates were normally optimized between 0.5 and 2 Hz. Leveling problems were nonexistent with the vertical-engage scanners.

Processing and analysis of images was carried out using the offline portion of Digital Instruments software version 5.12r3. Before performing offline zoom, section, surface plot, and particle functions, images were initially flattened using first-order fitting to remove sample tilt. A first-order plane fit operation was also applied to images along the *X* and *Y* coordinates of each image. For determining size distributions of vesicles using particle analysis, normal threshold techniques were always used.

Asymmetric flow field fractionation coupled with multiangle light scattering

An asymmetric flow-field fractionator (AFFF) (the Eclipse) connected in series with a multiangle static light-scattering (MASLS) photometer (the Dawn Eos) (Wyatt Technologies, Santa Barbara, CA), was used to measure the shape and geometric dimensions of plain liposomes and liposomes encapsulating actin. During a typical experiment, the liposome dispersion was injected into the AFFF channel, where it was separated. The separated liposome dispersion eluent flowed into the MASLS photometer, which continuously measured the particles' size and shape as a function of time.

The multiangle laser photometer is temperature-controlled to within 0.1°C, and was maintained at 25°C for all MASLS measurements. The photometer is equipped with a 30-mW Gallium-arsenide diode laser that emits a vertically polarized beam with a wavelength of 690 nm in vacuum, which is scattered by the sample. The scattered light is collimated, and simultaneously detected by a fixed array of 18 transimpedance photodiodes, which span an angular region from 22.5° to 147°. The light scattering intensity profile was recorded as a function of time at a rate of one full profile every 1 s. Here, $Q = (4\pi n/\lambda_0)\sin(\theta/2)$ is the amplitude of the scattering wave vector, $n = 1.3316$ is the refractive index of the buffer solution, θ is the scattering angle, and $\lambda_0 = 690$ nm is the wavelength of the incident light beam in vacuum. In preparation for all AFFF/MASLS experiments, all glassware was carefully cleaned, while all mobile phases (G- and F-buffer) were thoroughly filtered through 0.1 μm filters.

Asymmetric flow-field fractionation is a chromatographic separation technique, which is capable of separating a solution of polydisperse particles, with sizes ranging from 1 nm–10 μm, using two orthogonal flow fields acting within a trapezoidal-shaped channel. The top of the channel is bounded by an optically transparent acrylic block, while the bottom is bounded by a 10,000 molecular weight cutoff polymeric membrane, Nadir (Millipore, Bedford, MA). For all experiments the channel thickness was fixed at 350 μm. One flow field, the channel flow (v_c), is parallel to the polymer membrane. The other flow field, the cross flow (v_x), is perpendicular to the membrane.

In the focus/inject mode of operation, the liposome dispersion is injected to the channel, where it is subjected to a cross flow of 3 ml/min and a channel flow of 0 ml/min for 3 min. Liposomes exposed to the cross flow accumulate toward the membrane surface, where they rapidly equilibrate via molecular diffusion and form into a thin ellipsoidal sample front. The ellipsoidal sample front is perpendicular to the channel flow. In the elution mode of operation, the ellipsoidal sample region is exposed to a channel flow of 1 ml/min and a cross flow of 1.5 ml/min, which linearly decreases to 0 ml/min in

a 30-min interval. The cross flow acts to retain particles longer in the channel, thus separating the dispersion based on particle size.

In a typical separation, small particles (<1 μm) elute from the channel first, while larger particles elute last. This is characterized by an exponential distribution of particles near the accumulation wall (membrane). In the hyperlayer mode of operation, the elution order is reversed. In this case, particles with diameters larger than ~1 μm elute first. For the experiments described in this article, a typical separation lasted 30 min.

Liposome, actin, and substrate preparations

Liposomes were prepared by extrusion in stainless steel-Teflon extruders using 0.4 μm polycarbonate membranes, all obtained from Avanti Polar Lipids (Alabaster, AL). The extrusion procedure has been described well elsewhere (e.g., Olson, et al., 1979; Hope, et al., 1985; New, 1990; Korgel et al., 1998). In short, 0.01 volume of K^+ ionophore dissolved in chloroform (25 mg/ml) was added to 0.99 volume of 20 mg/ml L-α-Phosphatidylcholine (PC), also dissolved in chloroform. This solution was dried in a round bottom flask by rotary evaporation of the solvents at 40°C for 4 h, to ensure complete removal of chloroform. The resultant dried PC/ionophore film was rehydrated in either G-buffer (for liposomes not containing actin) or in a solution of 0.4 mg G-actin dissolved in 745 μl G-buffer + 255 μl deionized H_2O (for liposomes containing actin).

Before liposome extrusion, rehydrated PC/ionophore solutions were vortexed vigorously for ~10 min to ensure even mixing. The aqueous lipid solutions were then extruded 15× back and forth through the membrane, to yield plain liposomes and liposomes encapsulating G-actin. In preparation for AFM imaging the liposome dispersions were diluted in G-buffer 20-fold for sample incubation on the AFM. For liposomes encapsulating F-actin, polymerization was induced throughout the aqueous core of liposomes encapsulating G-actin by adding 0.1 volume of 10X F-buffer (500 mM KCl, 20 mM $MgCl_2$, and 10mM ATP) to 0.9 volume of PC/ionophore solution and pipetting gently for ~5 min. After gentle mixing with the pipette, this solution was allowed to polymerize for ~1 h so that K^+ ions could permeate through the ionophores embedded in the liposome membrane from the outside solution. After 1 h, the F-actin liposome suspension was diluted 20-fold in F-buffer for sample incubation on the AFM. In preparation for AFFF/MASLS studies, plain liposomes and liposomes encapsulating G- and F-actin were injected into the AFFF channel undiluted using either G- or F-buffer as the mobile phase. All liposome suspensions were used immediately after their preparation.

For G-actin preparation, 0.4 mg G-actin was dissolved in 745 μl G-buffer + 255 μl deionized H_2O. For F-actin preparation, 0.1 volume of 10× F-buffer was added to 0.9 volume of 0.4 mg G-actin dissolved in 745 μl G-buffer + 255 μl deionized H_2O, pipetted gently for ~5 min, then allowed to polymerize for ~1 h. Both G and F-actin solutions were imaged undiluted on the AFM immediately after their preparation.

For substrate preparations, microscope coverglass slides obtained from Fisher Scientific (Pittsburgh, PA) were stored in 20 vol % HCl in EtOH. Slides were washed repeatedly with deionized H_2O, then dried thoroughly with contaminant-free commercial air duster. After drying, slides were affixed to AFM specimen disks obtained from Ted Pella, Inc. (Redding, CA) using commercial epoxy.

THEORY

Light scattering

The excess Rayleigh ratio R_θ is a convenient way of expressing the light scattered by a sample at a particular angle. The following expression represents the scattering due to particles, which is equal to the difference in scattering between the particles in solution and the buffer solution.

$$R_\theta = r^2\left(\frac{I_\theta - I_{\theta,\text{solvent}}}{I_o V}\right). \quad (1)$$

Here, r is the distance between the scattering volume and the detector, I_θ is the scattered intensity of the solution, $I_{\theta,\text{solvent}}$ is the scattered intensity of the solvent, I_o is the intensity of the incident beam, and V is the volume of the scattering medium. This definition of R_θ is very robust since it corrects for any stray light present in the scattering volume along with any fluctuations in laser power. The determination of the molecular weight and size of a monodisperse system of particles can be derived from the following expression proposed by Zimm (1948a,b) for a vertically polarized monochromatic light source:

$$\frac{R}{Kc} = MP(\theta) - 2A_2cM^2P^2(\theta). \quad (2)$$

Here, $K = 4\pi^2n^2(dn/dc)^2/(\lambda_o^4 N_A)$ is the optical constant of the liposome solution, N_A is Avogadro's number which is equal to 6.023×10^{23}, c is the concentration of the solute in solution, M is the molecular weight of the solute, $P(\theta)$ is the theoretically derived form factor which is a function of the size, shape, and structure of the particle, and A_2 is the second virial coefficient. Since Zimm's expression only takes into account single contacts between macromolecules, it is typically used to model particle scattering in dilute solutions.

This expression can be further simplified since the particle concentration and second virial coefficient are usually small numbers $\ll 1$. During the separation process the concentration of liposomes is $\sim 10^{-6}$ mg/ml. Therefore, Eq. 2 is transformed into:

$$\frac{R}{Kc} = MP(\theta). \quad (3)$$

When analyzing MASLS spectra, the use of this equation is justified since AFFF separates a polydisperse sample into monodisperse components, which then flow into and are measured by the MASLS photometer. Hence, for all intensive purposes each eluting fraction is considered monodisperse.

To measure the size and shape of eluting liposomes, values of K and c are not needed. Instead, Eq. 2 can be normalized using the scattering from the 90° light scattering detector, $R(90°)$, to yield:

$$\frac{R(\theta)}{R(90°)} \approx \frac{P(\theta)}{P(90°)}. \quad (4)$$

In our study, we fit the experimental MASLS spectra to the form factors listed in Table 1, to regress the characteristic dimensions for that particular geometry. Hence, we are able to deduce the shape and size of eluting liposomes by testing which shape factor provides the best fit to the experimental MASLS spectra.

TABLE 1 Form factors for various geometries

Geometry	Form factor*
Solid sphere	$P(Q) = \left(\frac{3}{Q^3R^3}(\sin(QR) - QR\cos(QR))\right)^2$
Hollow sphere	$P(Q) = \left(\frac{3}{Q^3(R_O^3 - R_i^3)}(\sin(QR_o) - QR\cos(QR_o) - \sin(QR_i) + QR_i\cos(QR_i))\right)^2$
Infinitely thin hollow shell	$P(Q) = \left(\frac{\sin(QR)}{QR}\right)^2$
Infinitely thin rod	$P(Q) = \frac{2}{QL}\int_0^{QL}\frac{\sin(x)}{x}dx - \left(\frac{\sin(QL/2)}{QL/2}\right)^2$
Infinitely thin disk	$P(Q) = \left(\frac{2}{Q^2R^2}\right)\left(1 - \frac{J_1(2RQ)}{RQ}\right)$
Circular cylinder	$P(Q) = \int_0^{\pi/2}\left(\frac{\sin((QL/2)\cos(x))2J_1(QR\sin(x))}{(QL/2)\cos(x)QR\sin(x)}\right)^2\sin(x)dx$
Ellipsoidal of revolution	$P(Q) = \int_0^{\pi/2}\left(\frac{\sin^2\left(Q\sqrt{a^2\cos^2(x) + b^2\sin^2(x)}\right)}{Q^4(a^2\cos^2(x) + b^2\sin^2(x))^2}\right)\cos(x)dx$

R, Vesicle radius; R_o, Vesicle outer radius; R_i, Vesicle inner radius; L, Vesicle length; $J_1(x)$, Bessel function of the first order; a, Vesicle major semiaxis; and b, Vesicle minor semiaxis.
*See van Zanten (1996) for more information.

RESULTS

G-actin and F-actin imaged in respective buffers

Fig. 1 shows AFM images in fluid-tapping mode of actin adsorbed to a glass coverslip under different ionic strength conditions. The imaging, collected in G-buffer (Fig. 1 *A*) and F-buffer (Fig. 1 *C*) was done to study the behavior of actin on an AFM slide under buffers that would normally induce actin into respective monomeric (G-actin) and polymeric (F-actin) forms in solution. Sample pucks with cleaned and dried glass coverslips fixed to them were placed on the AFM scanner and incubated for ~10 min with either 50 μl of G-actin

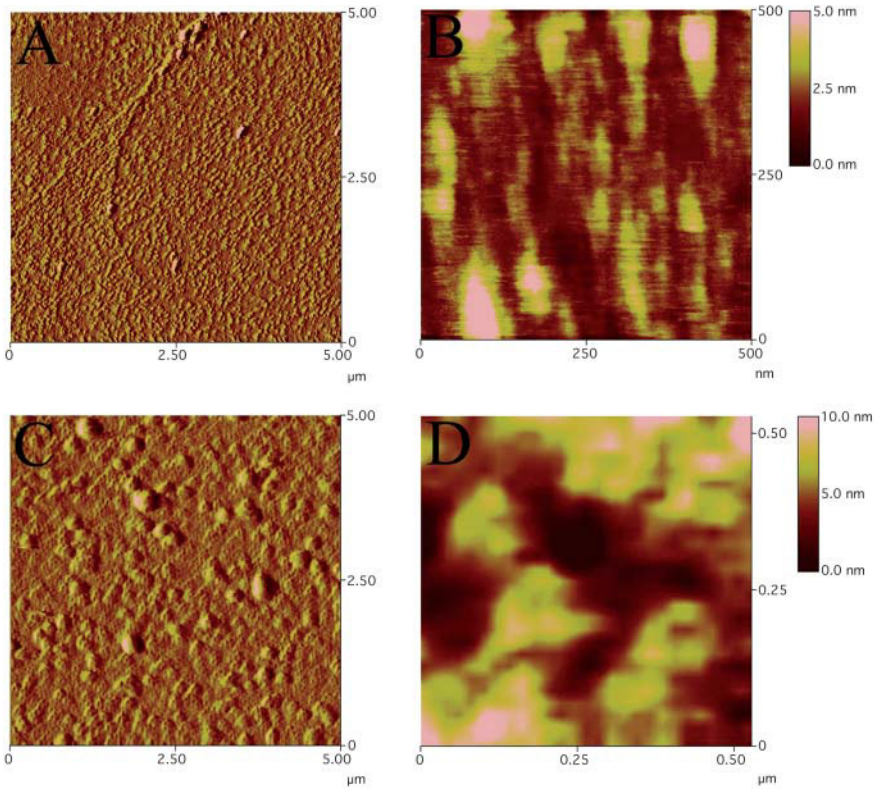

FIGURE 1 AFM fluid-tapping mode images capturing actin under different ionic strength conditions, taken at 0.8 Hz and 256 × 256 samples/line. The images were collected in G-buffer (*A*) and F-buffer (*C*) with the intent to image G-actin and F-actin respectively, and are presented in amplitude mode. *B* and *D*, presented in height mode, are offline zooms of the height data associated with *A* and *C* and show a more detailed view of the respective aggregates. The slow scan direction of scan *A* and *B* was top to bottom whereas for *C* and *D* it was bottom to top; for all scans shown, the line scan direction was trace (*right to left*).

solution or 50 μl of G-actin solution that had been previously incubated for 1 h in a 9:1 volume ratio with polymerization buffer (see the Materials and Methods section). A standard AFM O-ring was placed on the coverslip before incubation. After 10 min, excess fluid was pipetted off delicately to leave a wet residue behind on the coverslip. The fluid cell was then immediately loaded and the respective buffer (G- or F-buffer) was allowed to flow over the coverslip gently, which in effect prevented the sample on it from completely drying out for any period of time.

Fig. 1 *A* clearly distinguishes aggregates of actin monomers adsorbed evenly across the sample surface; the size ranges of actin aggregates in G-buffer are, on average, $\leq$14.5 nm high and $\leq$40 nm in diameter, and for actin in F-buffer, $\leq$46 nm high and $\leq$360 nm in diameter. Table 2 gives complete size distributions of the actin in different ionic strength buffers. In general, actin aggregates had larger dimensions in F-buffer versus G-buffer. Analysis of the size distribution of actin aggregates in G-buffer indicate as many as approximately four monomers stacked on top of one another, and as many as approximately 35 monomers stuck together laterally in the *x*- and *y*-directions; in F-buffer, the images indicate that aggregates comprise up to approximately 11 monomers stacked on top of one another, and up to approximately 90 stuck together laterally.

Actin tends to aggregate on glass surfaces if the pH of the solution, which is 8 in our case, is more than the pI of actin, which is ~5 (Sheterline et al., 1995). When this happens, actin assumes a net positive charge. Hence actin aggregates form on the glass surface due to the electrostatic attraction between the positively charged actin and the negatively charged glass surface. For all experiments, actin was always imaged in liquid with a pH of 8. In all cases, actin formed aggregates. The degree of aggregation was mediated by the ionic strength of the actin imaging solution. In the presence of F-buffer, G-actin is converted into F-actin. It is known that high ionic strength solutions (F-buffer) shield the surface charges on individual monomers, which allows them to self-assemble into actin filaments in bulk solution. In the case of imaging actin adsorbed to glass surfaces exposed to F-buffer, the initial number of actin monomers that adsorb to the glass surface is always less than if it were imaged in G-buffer. As the ionic strength is increased, the positively charged cations K^+ and Mg^{2+} shields both the negative surface charge on the glass and the positive charge on the actin monomer surface, thus lowering the degree of electrostatic attraction between the actin monomers in solution and the glass surface. However, the initial actin aggregates that form act as nucleation sites for the recruitment of additional actin monomers from the bulk. These actin nucleation sites lead to the formation of large aggregates due to charge shielding between actin monomers in the aggregate and monomers in the bulk. Hence actin imaged in high ionic strength buffers always form aggregates that have larger dimensions than those imaged in low ionic strength buffer.

Fig. 1 *C*, a scan of actin in F-actin forming conditions, shows the largest aggregates with sizes up to 46-nm high, 500-nm long, and 360-nm wide and no evidence of monomers forming filaments. Actin, whether monomeric or filamentous before incubation on the coverslip, immediately aggregated in both buffer solutions when those buffer solutions were placed onto the glass coverslip. Fig. 1, zooms *B* and *D*, are presented in height mode and were developed offline from height data directly associated with *A* and *C*. They show a more detailed view of the actin aggregates. Fig. 1 *B* is very interesting since it shows the presence of actin filaments adsorbed onto the glass surface.

TABLE 2 Size distributions of G-actin in G- and F-buffer

Dimensions	Mean	Minimum	Maximum	Sigma
G-actin in G-buffer, number of samples = 436				
Height (nm)	3.2	2.4	14.5	0.8
Area (nm^2)	844.0	24.6	16206.0	1268.0
Diameter (nm)	27.7	5.6	143.7	17.6
Length (nm)	43.0	7.0	222.1	32.5
Width (nm)	18.7	7.0	90.8	10.8
G-actin in F-buffer, number of samples = 38				
Height (nm)	15.4	10.2	46.3	7.1
Area (nm^2)	13453.0	24.2	103450.0	19564.0
Diameter (nm)	100.1	5.6	362.9	84.4
Length (nm)	130.4	7.0	499.2	111.6
Width (nm)	85.8	7.0	355.6	75.8

Plain liposomes imaged in G-buffer and F-buffer

Simple liposome dispersions were investigated with AFM at a 20-fold dilution from a stock solution consisting of 20 mg/ml PC and 0.2 mg/ml K^+ ionophore. Plain PC liposomes were imaged in G-buffer and F-buffer.

Because glass possesses a negative charge, we expected many initially adsorbed cationic liposomes to quickly collapse and form stacks of lipid bilayers on the coverslip in the first minutes of imaging. We noticed always after ~15 min of imaging that large areas of the coverslip were often covered by a smooth lipid film, comprised of either a single bilayer or multiple bilayers stacked on top of one another. When multiple bilayers were present, the surface usually did not appear smooth, as scattered lipid bilayer patches rested on top of a layer that was smoother overall. After 15 min, we rarely noticed any more lipid spreading from liposomes within the images. For all liposome images shown, liposomes are either absorbed to the glass or ultimately resemble flattened circular domes in both the height and amplitude data.

Fig. 2 shows AFM images capturing plain PC / potassium ionophore liposomes (Le). Liposomes collected in G-buffer are shown in *A* and in diluted F-buffer are shown in *B*. The majority of liposomes in these two images appear regularly spherical and not deformed. Liposomes imaged in F-buffer *B* are, on average, much larger in size. In *A*, the mean diameter,

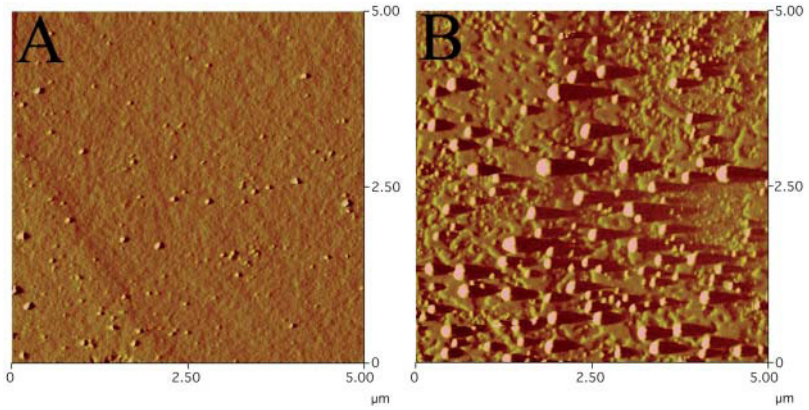

FIGURE 2 AFM fluid-tapping mode images capturing plain PC/potassium ionophore liposomes (Le), taken at 1 Hz (*A*) and 0.5 Hz (*B*), both with 256 × 256 samples/line. The images, collected in G-buffer (*A*) and F-buffer (*B*), are presented in amplitude mode. The slow scan direction of each scan was top to bottom, and the line scan direction was trace (*right to left*).

length, and width were 49, 67, and 38 nm, respectively. Some liposomes present were as large as 90 nm in diameter, up to 120 nm in length, and up to 75 nm in width. The height of these liposomes only ranged from 2.5 to 15.1 nm, which indicates that they were either very strongly adsorbed or possibly close to rupture. As can be seen, liposomes imaged in F-buffer are on average much larger in size, with mean diameter, length, and width of 110, 190, and 65 nm, with a maximum diameter, length, and width of 325, 615, and 160 nm, respectively. The height of the F-buffer liposomes ranged from 16 to 50 nm, indicating weaker adsorption. The complete size distributions of liposomes in Fig. 2, *A* and *B*, are found in Table 3.

The size difference between adsorbed PC liposomes in different buffers is due to a combination of factors. In G-buffer, adsorbed vesicles appear extremely small and flattened. The top of each vesicle is still evident with the remainder of the bilayer being adsorbed completely onto the glass surface. It should be noted that Reviakine and Brisson (2000) observed similar features under different experimental conditions and made the distinction that these features are not adsorbed liposomes but rather single-bilayer disks formed after introduction to the coverslip. In low ionic strength buffers there is a strong electrostatic attraction force between the positively charged liposome and the negatively charged glass surface. Hence in these buffers liposome adsorption to the glass is extremely strong; this gives rise to adsorbed liposomes with small diameters and heights. The majority of the lipid bilayer comprising these liposomes adsorbed onto the glass surface with only a small percentage of the original lipid appearing as a highly truncated spheres. In F-buffer, the increased ionic strength shields the surface charge on both the liposome and glass surfaces, which decreases the electrostatic attractive force between these two surfaces. Hence liposomes imaged in F-buffer are weakly adsorbed to the glass surface, and appear larger than liposomes imaged in low ionic strength G-buffer. Note that the presence of K^+ ionophore in the vesicle membrane eliminates the osmotic pressure gradient due to K^+ between the inside of the vesicles and the bulk fluid. The presence of Mg^{2+} ions has a negligible effect on vesicle shrinkage because of its low concentration in solution.

TABLE 3 Size distribution of plain liposomes in G- and F-buffer

Dimensions	Mean	Minimum	Maximum	Sigma
Liposomes in G-buffer, number of samples = 31				
Height (nm)	5.9	2.5	15.1	3.3
Area (nm^2)	2230.4	95.4	6198.9	1601.6
Diameter (nm)	49.3	11.0	88.8	20.2
Length (nm)	67.1	13.8	120.8	27.2
Width (nm)	38.4	13.8	73.8	16.0
Liposomes in F-buffer, number of samples = 52				
Height (nm)	25.7	16.1	48.7	7.1
Area (nm^2)	13531.0	95.4	82492.0	16672.0
Diameter (nm)	111.4	11.0	324.1	69.4
Length (nm)	193.1	13.8	615.5	136.3
Width (nm)	64.5	13.8	157.1	33.8

Fig. 3 shows the results of offline image processing that was performed on a single plain PC/potassium ionophore liposome adsorbed on a glass coverslip in G-buffer. The original scan of this liposome was in height mode. The liposome's height profile is ~45 nm, and adsorbed to the sample surface it has an apparent length (in its long axis) of ~150 nm and width (in its short axis) of ~95 nm. Because of the difference in observed length and width of this liposome, it may have stretched due to interaction with the AFM tip, which could have caused it to adsorb more to the sample surface along the long axis. The greater height of this liposome compared to Table 3 size distribution data indicates it was more weakly adsorbed than most vesicles imaged in G-buffer as seen in Fig. 2 *A*. The vesicle stretching evident in Fig. 3 is likely a result of the liposome bilayer's high flaccidity–because there is no cytoskeleton in the liposome, the liposome is generally deformable and floppy (Thomson et al., 2000). Section analysis (*A*) and a three-dimensional surface plot (*B*) both show this liposome's bilayer surface to be very smooth and regular.

Fig. 4 shows the results of the offline image processing that was performed on a plain PC/potassium ionophore liposome in F-buffer. The original scan of this liposome was

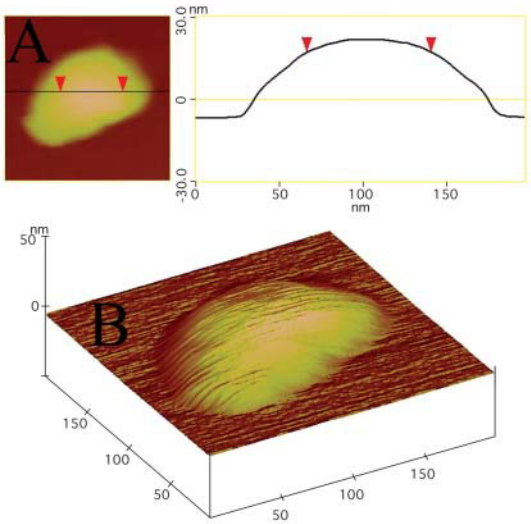

FIGURE 3 Offline image processing of an AFM fluid-tapping mode image capturing a representative plain PC/potassium ionophore liposome in G-buffer. The original scan of this single spherical liposome was captured in height mode, had a scan size of 400 × 400 nm, a 1-Hz scan rate, a top-to-bottom slow scan direction, a trace (*right to left*) line scan direction, and was 256 × 256 samples/line. Using offline software, the liposome was zoomed in on further, then a section analysis was completed (*A*) and a three-dimensional surface plot was developed (*B*).

in height mode. This liposome's height profile is ~55 nm (within the range of the size distribution data), and adsorbed to the sample surface it has an apparent width (in its short axis) of ~150 nm and length (in its long axis) of ~300 nm. More vesicle stretching is evident in this sequence and again

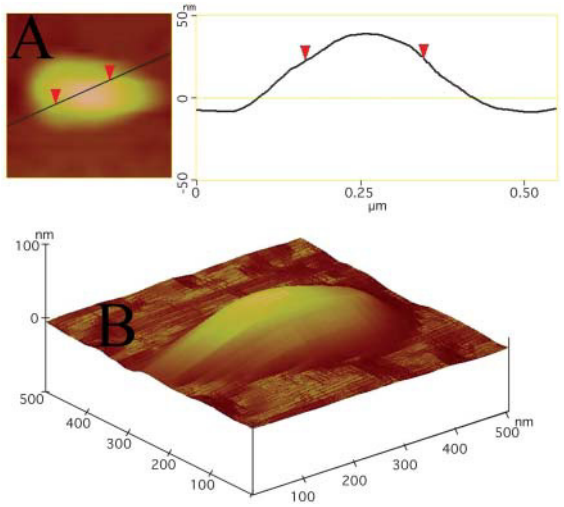

FIGURE 4 Offline image processing of an AFM fluid-tapping mode image capturing a representative plain PC/potassium ionophore liposome in F-buffer. The original scan of this single spherical liposome was captured in height mode, had a scan size of 5 × 5 μm, a 1-Hz scan rate, a top-to-bottom slow scan direction, a trace (*right to left*) line scan direction, and was 256 × 256 samples/line. Using offline software, the liposome was zoomed in on further, then a section analysis was completed (*A*) and a three-dimensional surface plot was developed (*B*).

directly results from the flaccid nature of the liposome bilayer. Because of the difference in observed length and width of this liposome, it may have stretched due to interaction with the AFM tip, which could have caused it to adsorb more to the sample surface along the long axis. Since this liposome is bigger than the one shown in Fig. 3, it could have been stretched out more along the long axis. However, because this liposome imaged in F-buffer is larger than it would have been under G-buffer conditions, it possibly stretched more. After performing an offline zoom of the liposome, a section analysis (*A*) and a three-dimensional surface plot (*B*) were completed and compare well qualitatively to Fig. 3, *A and B*, in that the vesicles are shaped similarly. Dimensions were ultimately larger in the liposomes imaged in F-buffer.

Liposomes encapsulating G-actin imaged in G-buffer

An image capturing plain PC/potassium ionophore liposomes encapsulating G-actin is shown in Fig. 5. The height scale of this figure is set high to clearly see the largest features, but there were two overall distributions of vesicles seen—those ones with large height (~60 nm) and those with very small height (~10 nm). The larger features had a mean height of 60 nm, a mean diameter of 135 nm, and mean length and width of 230 and 80 nm. The larger features may not even be single liposomes; since they show deformation from a spherical shape, they could represent aggregates of liposomes that have fused together or formed adhesive bonds. The smaller features had a mean height of 6.3 nm, a mean diameter of 73 nm, and mean length and width of 133 and 42 nm. These smaller features represent the most significant population in this image and are most likely all

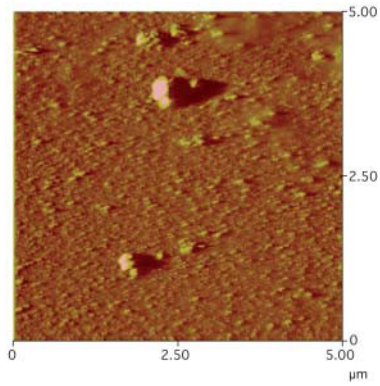

FIGURE 5 AFM fluid-tapping mode image capturing PC/potassium ionophore liposomes encapsulating G-actin, taken at 1 Hz and 256 × 256 samples/line. The image, collected in G-buffer, is presented in amplitude mode. Liposomes in these images are comprised of two distinct populations, where the larger liposomes appear irregular and the smaller liposomes appear regular. The slow scan direction was top to bottom, and the line scan direction was trace (*right to left*).

single liposomes encapsulating G-actin. Interestingly, the shapes of these adsorbed liposomes do not appear spherical, but rather disk-shaped. It is possible some of these liposomes could be mistaken for aggregates of G-actin monomers that remained unencapsulated during preparation, but we do not believe this is the case, since mean feature sizes for this image were all significantly larger than mean feature sizes of plain G-actin imaged in G-buffer (see Fig. 1, *A* and *B*). Several of the large liposomes in these images appear to have irregularities pronounced directly on the vesicle bilayer. The largest liposomes in the figure indicate deformation from a spherical shape, but they could merely be several liposomes fused together. G-actin self-polymerization inside the liposomes cannot be ruled out in these larger vesicles. Smaller liposomes and possibly G-actin aggregates exist in the figure and could be seen more clearly with a very decreased height scale.

The fact that there are fewer large irregular shaped liposomes in this image as compared to Fig. 2, *A* and *B*, lead us to believe the most prevalent liposomes on the surface for these samples are the ones with ~10 nm heights. Size distributions taken (see Table 4) give for the smaller distribution a mean diameter of ~70 nm, which is larger than the G-actin aggregate mean diameter given in Table 2. Overall, this smaller distribution is likely more represented by liposomes and not G-actin aggregates, but a few of the smallest features could be G-actin aggregates.

To better investigate the apparent bilayer irregularities of liposomes encapsulating G-actin at large scans, a capture of an individual liposome aggregate was attained in height mode and is shown in Fig. 6. The original scan of this single irregularly shaped liposome displays similar vesicle stretching to the previous liposomes examined, with a height profile ~115 nm, as well as an apparent width (at its shortest) of ~270 nm and length (at its longest) of ~470 nm while adsorbed to the sample surface. Overall, it seems likely that most G-actin encapsulated liposomes are disk-shaped, while a small percentage consist of liposome aggregates with irregular protrusions extending from the aggregate surface. With offline software, the liposome was zoomed in on further and section analysis (*A*) and a three-dimensional surface plot (*B*) performed. Fig. 6 *B* shows in great detail the presence of a very bumpy and irregular surface profile across the liposome aggregate, while (*A*) shows this liposome's bumpy surface to also be different from the much smoother curves shown in Figs. 3 *B* and 4 *B*. The presence of irregularly shaped G-actin liposome aggregates leads us to postulate that G-actin self-assembles on the inner surface of the cationic liposome. This yields protrusions and bumps on the otherwise smooth spherical liposome surface.

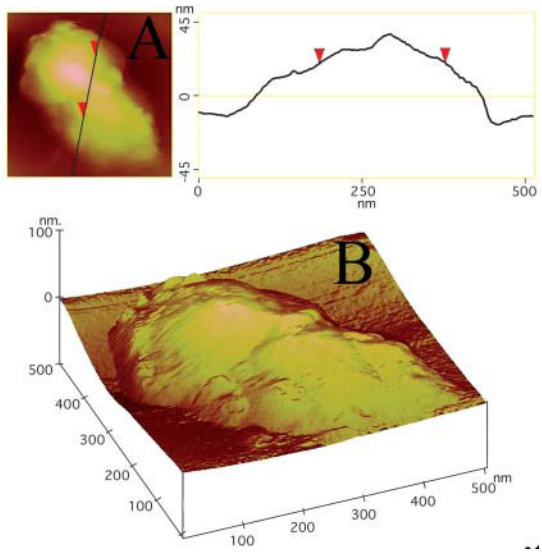

FIGURE 6 Offline image processing of an AFM fluid-tapping mode image capturing an irregular PC/potassium ionophore liposome encapsulating G-actin. The image, originally collected in G-buffer, was in height mode. The original scan of this single irregularly shaped liposome had a scan size of 1×1 μm, a 0.8 Hz scan rate, a top-to-bottom slow scan direction, a trace (*right to left*) line scan direction, and was 256×256 samples/line. Using offline software, the liposome was zoomed in on further, then a section analysis was completed (*A*) and a three-dimensional surface plot was developed (*B*).

TABLE 4 Size distributions of liposomes encapsulating actin in G- and F-buffer

Dimensions	Mean	Minimum	Maximum	Sigma
LeAcG in G-buffer, large irregular aggregates, number of samples = 12				
Height (nm)	19.9	10.8	62.7	14.312
Area (nm^2)	32695.0	286.1	272655.0	74162.0
Diameter (nm)	134.9	19.1	589.2	153.0
Length (nm)	233.1	30.9	965.3	255.4
Width (nm)	80.5	13.8	340.5	88.1
LeAcG in G-buffer, small disk-shaped liposomes, number of samples = 10				
Height (nm)	6.3	4.3	9.3	1.7
Area (nm^2)	4759.9	1062.3	10797.0	3149.6
Diameter (nm)	73.2	36.8	117.3	26.5
Length (nm)	133.4	63.9	211.1	49.3
Width (nm)	41.9	20.1	62.2	13.6
LeAcF in F-buffer, number of samples = 63				
Height (nm)	4.2	2.4	17.4	3.1
Area (nm^2)	14542.0	4559.8	49982.0	13405.0
Diameter (nm)	125.2	76.2	252.3	53.2
Length (nm)	167.3	95.8	398.0	80.9
Width (nm)	109.5	81.2	215.5	40.5

Liposomes encapsulating F-actin imaged in F-buffer

Images in Figs. 7 and 8 capture representative PC/potassium ionophore liposomes encapsulating F-actin (LeAcF). It is evident that many different types of structures are formed during the polymerization process. Fig. 7 *A* indicates an overall vesicle transformation from a spherical geometry (in the case of plain liposomes imaged in both G- and F-buffer) to a disk-like geometry (in the case of G-actin liposomes) to

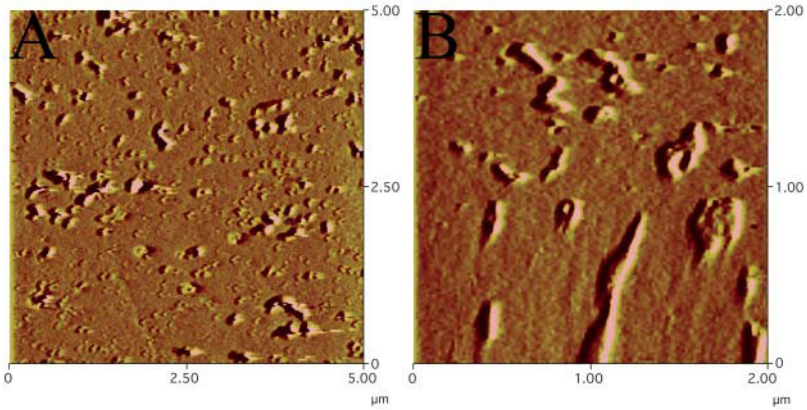

FIGURE 7 AFM fluid-tapping mode images capturing PC/potassium ionophore liposomes encapsulating F-actin (LeAcF), taken at 1 Hz and 256 × 256 samples/line. The images, collected in F-buffer, are presented in amplitude mode. Scan *A* shows mainly torus- and disk-shaped liposomes, while scan *B* shows horseshoe and tubular liposomes. The slow scan direction of each scan was top to bottom, and the line scan direction was trace (*right to left*).

finally torus, horseshoe, disk, and tubular geometries (in the case of F-actin liposomes). In Fig. 7 *A*, the mean diameter, length, and width of these liposomes were 125, 167, and 110 nm, respectively. Some liposomes present were as large as 250 nm in diameter, up to 400 nm in length, and up to 215 nm in width. The size distribution of these vesicles was measured and given in Table 4. Fig. 7 *B* shows encapsulated F-actin leading to other structures: long lipid tubules, horseshoe structures, and other irregularities. The sizes of the tubules in *B* ranged up to 750 nm in length and up to 400 nm in width, with similar heights to the liposomes in *A*. It is possible that in this scan area the vesicles were not well dispersed; however, we cannot discount the possibility of irregular shapes being formed in addition to the torus and horseshoe shapes.

Fig. 8 comprises a sequential series of AFM fluid-tapping mode images capturing LeAcF. The images demonstrate image reproducibility of LeAcF vesicles. They are collected in F-buffer and are presented in amplitude mode. Aside from slight cantilever drift due to mechanical vibration, the scans are nearly identical topographically. Of interest in these scans is the ~6-μm-long, ~80-nm-wide tubules formed (*lower left* of *A–D*) and evidence of torus or disk-shaped liposomes. The tubules could consist of bundles of

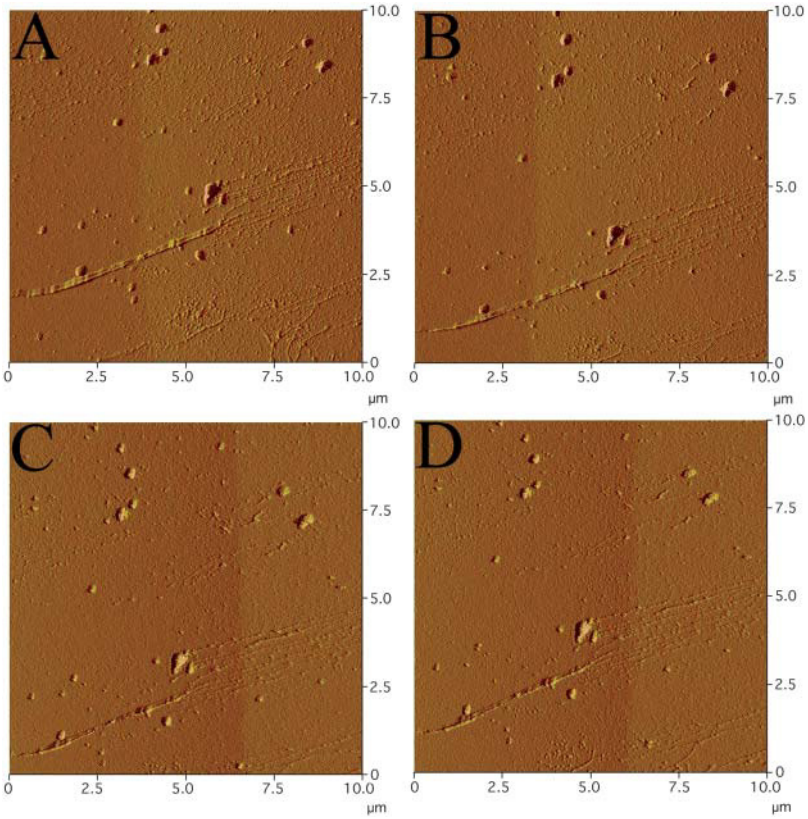

FIGURE 8 A sequential series of AFM fluid-tapping mode images capturing PC/potassium ionophore liposomes encapsulating F-actin (LeAcF), taken at 0.75 Hz and 512 × 512 samples/line. All scan sizes are 10 × 10 μm and line and slow scan directions are as follows: (*A*) trace and top to bottom, (*B*) trace and bottom to top, (*C*) retrace and top to bottom, and (*D*) retrace and bottom to top. The trace scan direction denotes right to left and the retrace scan direction denotes left to right.

unencapsulated actin filaments, or encapsulated actin filaments surrounded by a lipid bilayer. The torus-shaped vesicles have a depression in the center, as seen in many of the vesicles shown in the upper left center of *A–D* even at this 10-μm scanning range. Other less significant tubules had sizes ranging from 2- to 5-μm long and 20- to 60-nm wide.

LeAcF: a closer look

In Fig. 9 the offline image processing of an image capturing a LeAcF vesicle is shown. The original scan (*A*) of this single torus-shaped liposome was taken at 128 × 128 samples per line, which is a lower resolution than all previous images and correlates to the least amount of possible drift while capturing the image. The liposome's height profile is ~15 nm, and adsorbed to the sample surface it has an apparent width (in its short axis) of ~300 nm and length (in its long axis) of ~375 nm. If we assume that the liposome is lying on a single or stack of lipid bilayers, the 15-nm vesicle height profile could be attributed to the presence of an upper bilayer and a stack of actin: 4 nm contributes to the upper bilayer thickness, and the remaining 11 nm is due to the presence of encapsulated actin. If we assume an actin monomer occupies a 3.7 × 4 × 6.7 nm rectangular unit cell (Kabsch et al., 1990), we could have a stack of actin that is as much as three monomers high.

With offline software, Fig. 9, *B* and *C*, was compiled. The absolute depth of the depression is ~15 nm, whereas the absolute height difference between the ''surface'' and the outer edge of each peak is ~7 nm. The surface plot (Fig. 10) clearly shows the center depression in the torus shape and also shows two resultant ''peaks'' on either side. Clearly, this liposome has been smothered to the point where the surrounding topography is almost as high and is thus surrounded by what is likely two PC monolayers stacked on top of one another. The bottom of the depression could be the glass coverslip.

Light scattering of liposomes encapsulating G- and F-actin

Fig. 11 shows the MASLS spectra of liposomes encapsulating G-actin in G-buffer. MASLS spectra were fit to all of the form factors listed in Table 1. Of all the shape factor models that were fit to the data, the infinitely thin disk model fit the best, indicating with a high probability that the G-actin liposomes are indeed disk-shaped. The dashed lines show how well the thin disk model simulated the data. We noticed that application of the cylinder shape factor did not result in a good fit to the MASLS spectra, indicating to us that the G-actin-containing liposomes have an extremely large aspect ratio (i.e., disk radius/disk thickness ≫ 1). In addition, the thin shell and sphere shape factors did not fit the MASLS data. This suggests the absence of hollow shell and solid sphere particles in solution. Regressed radii at various points along the AFFF elution peak are shown in Fig. 12. It is evident that a dispersion of disk-shaped liposomes was formed, ranging from ~460 nm to ~600 nm in radius. This result shows the ability of G-actin to transform a liposome from an initially spherical shape (plain liposome in G- or F-buffer) into a thin disk. We must stress that in actuality the disk does have a finite thickness, since our AFM measurements show the presence of adsorbed disks with thickness ~6 nm. However, light scattering is not able to resolve this small dimension. To determine the actual thickness of this disk, we would have to resort to scattering techniques with smaller radiation wavelengths such as x-ray or neutron scattering. So while in actuality the disks are not infinitely

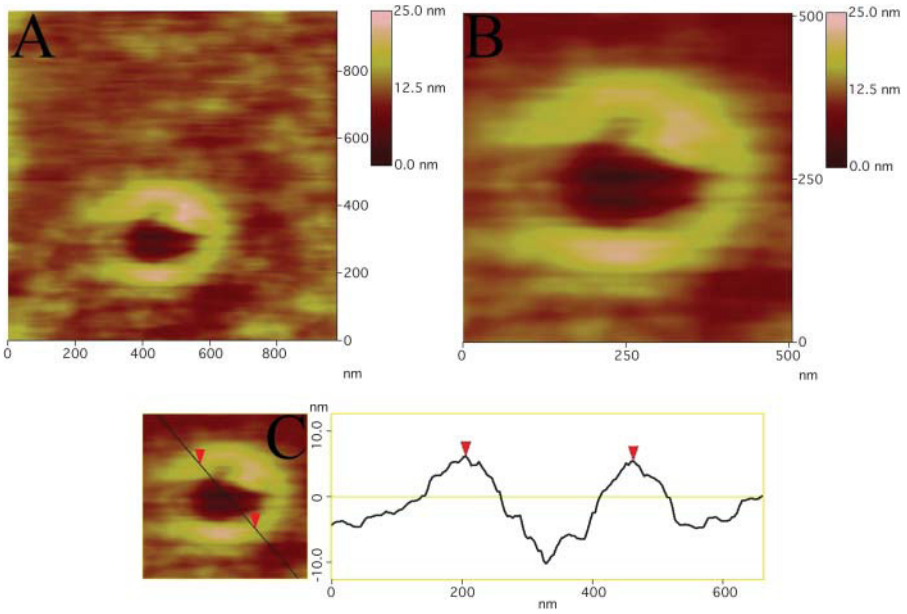

FIGURE 9 Offline image processing of an AFM fluid-tapping mode image capturing a representative PC/potassium ionophore liposome encapsulating F-actin (LeAcF). The image, originally collected in F-buffer, was in height mode. The original scan (*A*) of this single torus-shaped liposome had a scan size of 1 × 1 μm, a 0.5 Hz scan rate, a top-to-bottom slow scan direction, a trace (*right to left*) line scan direction, and 128 × 128 samples/line. Using offline software, the liposome was zoomed in on further (*B*), and a section analysis completed (*C*).

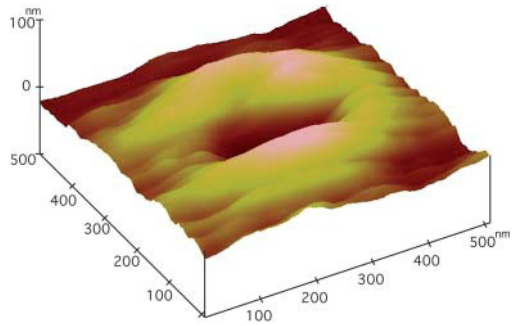

FIGURE 10 Surface plot of an AFM fluid-tapping mode image capturing a representative PC/potassium ionophore liposome encapsulating F-actin (LeAcF).

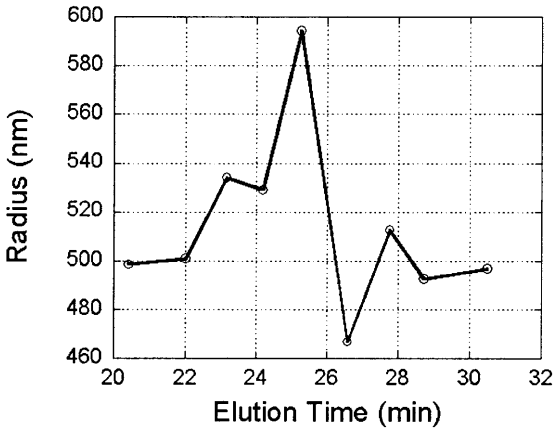

FIGURE 12 Elution profile of liposomes encapsulating G-actin in G-buffer. Fitting the light scattering spectra at each time slice to the infinitely thin disk form factor model generated this curve.

thin, we can be certain that the disk is thin such that the disk radius $\gg$ disk thickness.

Figs. 13 and 14 show the MASLS spectra of liposomes encapsulating F-actin in F-buffer. MASLS spectra were fit to all of the form factors in Table 1. It was found that both the thin disk and cylinder shape factors fit the data well, as is evident in the fits (dashed lines) shown in Figs. 13 and 14, respectively. The other shape factors did not fit the data, which indicates that the F-actin liposome dispersion is composed of cylindrical and disk-shaped objects. Fig. 15 shows the regressed radii derived from the infinitely thin-disk-shape factor applied to the MASLS data along the AFFF elution peak. The data indicates that the F-actin liposome dispersion has particles with radii which range from ~130 nm to 300 nm. Fig. 16 shows the regressed cylinder thickness and radii derived from applying the cylinder shape factor to the MASLS data along the AFFF elution peak. At short times, cylinders with small radii and large thickness (thin rods) elute from the AFFF channel. The initial data point is most probably due to eluting actin filaments since the regressed radius and thickness was ~5 nm and ~500 nm, respectively. Individual actin filaments have a radius of 7 nm (Sheterline et al., 1995). At an elution time of 19 min, the AFFF elution profile attains a minimum in the cylinder thickness. Thin disks elute from the AFFF channel with radii ~200 nm and thickness of ~13 nm. At long times $\geq$22 min, the elution profile reaches steady state with respect to the cylinder thickness (~50 nm) and the cylinder radius (~300 nm). Overall it is evident that the F-actin-containing liposomes are composed of three different populations of shapes possessing cylindrical symmetry namely: thin rod, thin disk, and disk. Comparing Figs. 15 and 16, it is evident that both models predict the same values of the disk radius at 19.3 and 20.2 min. As the elution time is

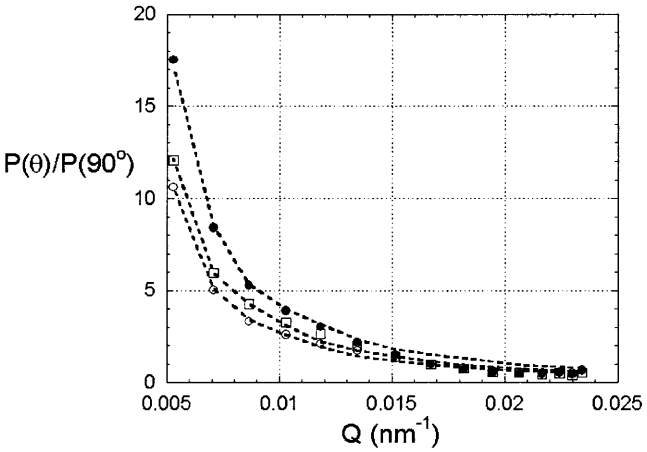

FIGURE 11 Normalized light scattering spectra of liposomes encapsulating G-actin in G-buffer taken at three different elution times: 23.2, 25.3, and 28.7 min, represented by unfilled circles, squares, and filled circles, respectively. The dashed lines represents fits to the data using the infinitely thin disk form factor model.

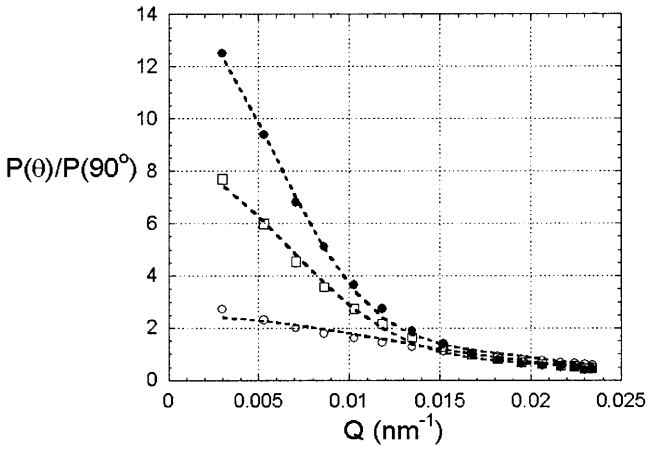

FIGURE 13 Normalized light scattering spectra of liposomes encapsulating F-actin in F-buffer taken at three different elution times: 18, 20.2, and 23.3 min, represented by unfilled circles, squares, and filled circles, respectively. The dashed lines represents fits to the data using the infinitely thin disk form factor model.

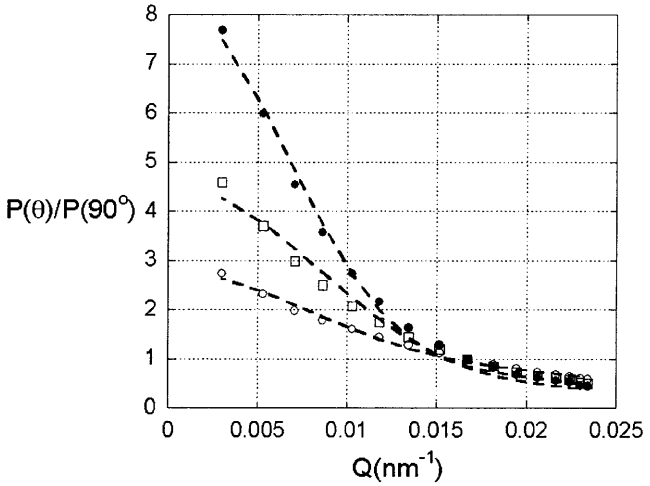

FIGURE 14 Normalized light scattering spectra of liposomes encapsulating F-actin in F-buffer taken at three different elution times: 18, 20.2, and 23.3 min, represented by unfilled circles, squares, and filled circles, respectively. The dashed lines represents fits to the data using the cylinder form factor model.

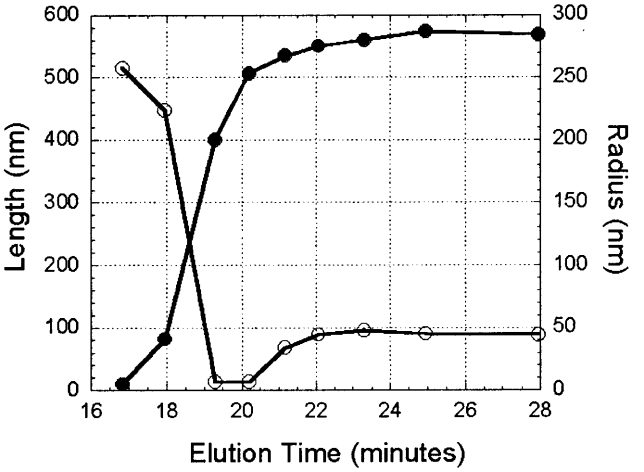

FIGURE 16 Elution profile of liposomes encapsulating F-actin in F-buffer. Fitting the light scattering spectra at each time slice to the cylinder form factor model generated this curve. The filled circles represent the cylinder radius, whereas the unfilled circles represent the cylinder length.

increased above this point, the predicted radius regressed from both the cylinder and infinitely thin disk shape factors diverge. Since the infinitely thin disk model cannot physically account for the thickness of disks this divergence in the predicted radii is reasonable.

DISCUSSION

G- and F-actin adsorption

Our results show the presence of filamentous actin adsorbed to a glass surface (Fig. 1 *B*), when a solution of G-actin was imaged in G-buffer. In bulk solution, G-actin in G-buffer is unable to self-assemble into F-actin without the addition of monovalent or divalent cations in high concentration. However, one group has observed the polymerization of G-actin on the surface of positively charged supported bilayers and liposomes (Rioux and Gicquaud, 1985; Laliberte and Gicquaud, 1988). Their findings are similar to ours with the exception that, in our case, G-actin polymerizes on a negatively charged surface. This observation leads us to postulate that G-actin is able to self-assemble into F-actin on both negatively and positively charged surfaces. We hypothesize that the surface functions to aid the sequestration of monomers from the bulk and to guide their self-assembly into filaments.

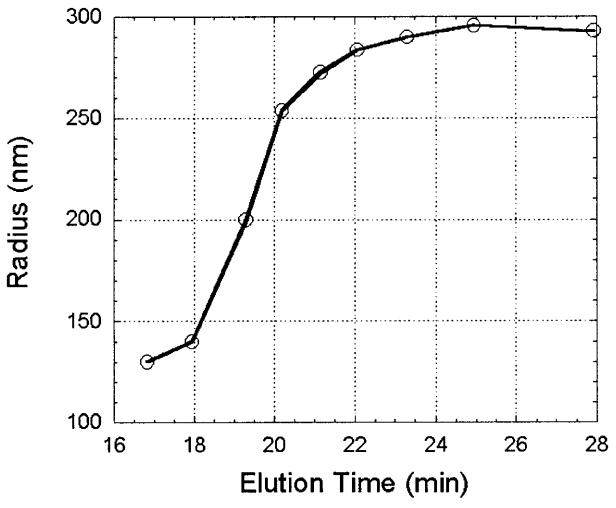

FIGURE 15 Elution profile of liposomes encapsulating F-actin in F-buffer. Fitting the light scattering spectra at each time slice to the infinitely thin disk form factor model generated this curve.

In contrast, AFM imaging of G-actin in F-buffer reveals the absence of actin filaments on the glass surface. Note that G-actin in F-buffer (F-actin) forms a three-dimensional network, which extends throughout the entire sample. Hence, during scanning, we assume that the AFM tip in effect sweeps the connected three-dimensional network away from the glass surface. Therefore, AFM imaging does not show the presence of F-actin on the surface. AFM imaging would show the presence of actin filaments in F-buffer if the sample were dried and imaged in air.

Plain liposome adsorption

It is assumed that the electrostatic interaction between a phosphatidylcholine liposome and a glass surface is a crucial factor in determining the behavior of liposomes while being imaged with AFM (Egawa and Furusawa, 1999). The addition of metal cation may lead to overcompensation of the surface charge and change it from a negative value to a slightly positive value. In our

experiment, the glass substrate's surface charge played a major role in liposome adsorption in both buffers G and F. This charge possibly could have been offset more when imaging in F-buffer by thoroughly rinsing the glass with F-buffer instead of pure water, as a charge pre-shielding of sorts before incubation with the liposome dispersion. Thus, it is possible the difference in vesicle size between plain liposomes imaged in G- and F-buffer could have been greater with this varied substrate preparation, with G-buffer vesicles remaining nearly the same size (rinsing the glass with G-buffer would not shield the glass's negative charge as significantly due to the low ionic strength of the buffer) and F-buffer vesicles adsorbing even more weakly and retaining their size even more closely to conditions in bulk solution.

The presence of divalent alkali cations has a dramatic effect on the surface potential and ion distribution of a negatively charged surface such as glass. In particular, Ca^{2+} and Mg^{2+} bind to phospholipids and provide membranes with positive charges. Even when the bulk concentration of Mg^{2+} is much smaller than that of K^+ as in F-buffer, the surface may have a much higher local concentration of Mg^{2+} than K^+ (Israelachvili, 1992). It is perhaps more accurate to say that for liposomes imaged in F-buffer, charge shielding of glass's electrostatic contribution for weaker liposome adsorption was as much a function of the presence of K^+ as it was of Mg^{2+}.

Liposomes encapsulating G-actin

Actin, the major protein of muscle cells, was chosen for study here because it exists in the cytoplasm of all eukaryotic cells and is one of the most important components of intracellular structures such as stress fibers, and the actin cortex. To our knowledge, AFM imaging and MASLS of small (<500 nm diameter) unilamellar liposomes encapsulating actin have not been previously studied. Our study can serve to partially address the effect of confining F-actin inside small unilamellar liposomes, which are smaller than the persistence length of individual actin filaments. All previous studies on actin-encapsulating liposomes focused on giant liposomes with sizes ranging from several to a few hundred microns.

Our study of LeAcG does not compare well to other actin/liposome studies in part because G-actin in GLs was always investigated at temperatures where it was known actin would not self-polymerize (~0°C), whereas our study was conducted at room temperature and self-polymerization cannot be ruled out. In addition, the size of our liposomes (~400-nm diameter) was much smaller than the smallest GL studies. Nonetheless, many studies reported shapes that were usually spherical (Cortese et al., 1989; Miyata and Hotani, 1992). In contrast, our G-actin-containing liposomes assumed disk-like shapes. Specifically, our AFM measurements indicated the presence of disk-like objects with a mean diameter of ~73 nm and a mean height of ~6 nm (Table 4). To corroborate these observations, MASLS measurements indicate that G-actin liposomes in bulk solution assume a thin disk geometry, with diameters ranging from ~920 nm to ~1200 nm. We were not able to experimentally determine the thickness of these liposomes. However, MASLS allows us to deduce from fits to the data, applying both the infinitely thin disk and cylinder shape factor models, that G-actin liposomes have a disk radius which is much larger than the disk thickness. This leads us to conclude that LeAcGs are highly adsorbed onto the glass surface during AFM imaging, which causes them to appear as highly truncated disks.

One possible explanation for the difference in our observed LeAcG structure and that observed in GLs stems from the fact that our liposomes (~400 nm diameter) have a larger surface area-to-volume ratio versus giant liposomes encapsulating G-actin. This leads to the possibility of G-actin self-assembling inside of the smaller liposomes, since there is an increased probability of G-actin interacting with the positively charged internal leaflet of the liposomes. This result is in agreement with observations that show the presence of a charged bilayer is sufficient to induce actin polymerization on its surface (Rioux and Gicquaud, 1985; Laliberte and Gicquaud, 1988).

Our observations support the claim that monovalent or divalent cations are not necessary to polymerize G-actin into F-actin. This raises some very interesting possibilities when applied to the spatial distribution of actin in eukaryotic cells. First, the presence of a highly dense actin cortex localized on the inner leaflet of the cell membrane can be explained by the ability of the cell membrane to guide actin polymerization on its surface, whereas the sparse population of vesicular assemblies in the bulk cytoplasm tends toward generating nonlocalized three-dimensional actin networks with larger pore sizes versus those in the actin cortex. In our studies of G-actin-containing liposomes, we observe the formation of a few highly irregular vesicular assemblies. These assemblies were not observed when plain PC liposomes were imaged in G-buffer. Hence we can deduce that the presence of G-actin induces the formation of these irregular structures. These structures are most probably large aggregates of G-actin-containing liposomes. It must be noted that the most populous structure on the glass surface consisted of highly adsorbed disk-shaped G-actin liposomes. The resultant aggregates may have many internal lipid lined compartments, which contributes to its highly irregular shape.

Liposomes encapsulating F-actin

One of the major differences between our liposomes encapsulating F-actin and many of the GL studies, other than size of vesicle, is in the actin polymerization method. Our method used K^+ ionophore, which was added to our lipid bilayer composition to facilitate the transport of K^+ ions into our LeAc samples for polymerization. Many of the

GL studies, however, initiated a temperature jump to induce G-actin polymerization; for example, Miyata and Hotani (1992) prepared their vesicles with actin at a low temperature (10°C) then heated to a higher temperature (30°C) so Ca^{2+} ions could permeate through the vesicle's membrane and polymerize the actin. This altered the membrane fluidity of their vesicles, which could have influenced the shape changes they observed in their GLs. Initially, spherical G-actin-containing giant liposomes transformed via actin polymerization into dumbbell and disk shapes. The actin in these structures was localized near the inner leaflet of the liposome. The disk shapes we observed via AFM were of similar geometry to their disk shapes. However, we never observed a dumbbell-shaped liposome. MASLS and AFM measurements on F-actin containing liposomes support the presence of disk-shaped liposomes observed by other groups.

Before Miyata and Hotani's study, Cortese et al. (1989) showed that GLs changed their shape from spherical to irregular upon actin polymerization inside the vesicles, due to a heterogeneous distribution of actin filaments. This was explained by suggesting discrete nucleation sites for polymerization, where filaments grown from these sites acted as primers for the formation of still larger filament bundles, which led to a heterogeneous actin distribution as the initial distribution of nuclei was probably uneven. The system Miyata and Hotani reported was more regular after polymerization, possibly because the Ca^{2+} ions they used suppressed and slowed the polymerization process. They reported that actin polymerization in GLs initiated by introducing K^+ or Mg^{2+} ions caused liposome morphogenesis from an elongated form to an oblate ellipsoid. This is somewhat analogous to our disk-shaped vesicles, but again, the size of our vesicles prevents anything more than a qualitative comparison.

In the experiments Miyata and Hotani (1992) conducted, they observed no tendency of aligned filaments to form circular structures on their own without the liposomes. We observed similar phenomena in that G- and F-actin imaged on glass did not form circular structures.

Renault et al. (1999) studied the surface-induced polymerization of actin and showed that a nonpolymerizing G-actin solution could be induced to assemble into individual filaments on the surface of a positively charged lipid monolayer. This work could help explain the existence of actin filaments shown in Fig. 8, *A–D*. Since our glass surface was highly negatively charged, lipid bilayer(s) formed from the collapse of some liposomes in all of our captures. The existence of the lipid bilayer(s) could have easily supported G-actin assembly into long actin filaments with lengths in excess of 10 μm. We must stress that these structures could also be bundles of actin filaments encapsulated by a lipid bilayer. We also observed the presence of lipid tubules (Fig. 7 *B*), which were not observed by Miyata and Hotani (1992). These lipid tubules were shorter in length ($\sim$1 μm) and larger in width versus their actin filament counterparts (Sheterline et al., 1995). Tubules of this kind were observed by Hotani and Miyamoto (1990), with the exception that the GLs contained microtubules instead of actin. Our MASLS measurements support the presence of individual actin filaments, thin rods (tubules), thin disks, and disks in solution.

We can explain the formation of tubules by comparing the size of the liposome ($\sim$400 nm) to the persistence length of actin filaments ($\sim$0.5–15 μm) (Ott et al., 1993; Gittes et al., 1993; Isambert et al., 1995). When actin is polymerized in a confined space, with a characteristic diameter that less than actin's persistence length, it will adopt a rod-like shape. Hence we expect to observe rod-shaped tubules that are formed as a result of the protrusive growth of actin filaments inside of the liposome.

MASLS measurements show that actin polymerization inside initially thin-disk-shaped G-actin-containing liposomes with large aspect ratios (disk radius/disk thickness $\gg$1) induces a dramatic shape transformation into disks with aspect ratios of order 0.1. The fact that these liposomes change shape leads us to postulate that G-actin self-assembles inside of these disks. We further conclude that this shape transformation is not due to an osmotic pressure change. The presence of K^+ ionophores eliminates the osmotic pressure due to K^+ ions. There is a slight osmotic pressure gradient due to the presence of Mg^{2+} ions, which would shrink the liposomes marginally. However, the resultant F-actin-containing liposomes actually increase in volume. More studies need to be made to ascertain the spatial distribution of actin within the liposome. We do know from our AFM studies, however, that these liposomes highly adsorb to the glass surface. Therefore, Fig. 10 could be the remnants of an LeAcF that is in the last stages of the adsorption process, where most of the LeAcF bilayer has adsorbed onto the surrounding glass surface, and the resultant structure is the remaining actin matrix coated by a lipid bilayer. If this structure is indeed the actin matrix, it indicates that the actin matrix was localized around the outer periphery of the disk.

The existence of thin rods (tubules), thin disks, disks, and torus geometries leads us to postulate that actin is able to transform an initially spherical liposome (plain liposome in G- or F-buffer) into an infinitely thin disk (G-actin-containing liposome) and finally into thin rods, thin disks, disks, and torus-shaped liposomes (F-actin-containing liposomes). This leads us to postulate the importance of actin's ability to interact in concert with lipid bilayers to actively remodel the cytoskeleton in living cells.

Other studies of GLs encapsulating actin have probed the effects of shape instabilities due to a local softening of the actin cytoskeleton (Boulbitch et al., 2000), which could lead to morphogenesis. Again, since our vesicles are much smaller, morphological changes due to this issue remain unclear.

We acknowledge support from the National Science Foundation (BES 0196432), and the National Institute of Standards and Technology.

REFERENCES

Balashev, K., T. R. Jensen, K. Kjaer, and T. Bjørnholm. 2001. Novel methods for studying lipids and lipases and their mutual interaction at interfaces. Part I. Atomic force microscopy. *Biochimie*. 83:387–397.

Boulbitch, A., R. Simson, D. A. Simson, R. Merkel, W. Häckl, M. Bärmann, and E. Sackmann. 2000. Shape instability of a biomembrane driven by a local softening of the underlying actin cortex. *Phys. Rev. E*. 62:3974–3985.

Cortese, J. D., B. Schwab III, C. Frieden, and E. L. Elson. 1989. Actin polymerization induces a shape change in actin-containing vesicles. *Proc. Natl. Acad. Sci. USA*. 86:5773–5777.

Egawa, H., and K. Furusawa. 1999. Liposome adhesion on mica surface studied by atomic force microscopy. *Langmuir*. 15:1660–1666.

Gittes, F., B. Mickey, J. Nettleton, and J. Howard. 1993. Flexural rigidity of microtubules and actin filaments measured from thermal fluctuations in shape. *J. Cell Biol*. 120:923–934.

Häckl, W., M. Bärmann, and E. Sackmann. 1998. Shape changes of self-assembled actin bilayer composite membranes. *Phys. Rev. Lett*. 80:1786–1789.

Helfer, E., S. Harlepp, L. Bourdieu, J. Robert, F. C. MacKintosh, and D. Chatenay. 2001. Viscoelastic properties of actin-coated membranes. *Phys. Rev. E*. 63:021904.

Hope, M. J., M. B. Bally, G. Webb, and P. R. Cullis. 1985. Production of large unilamellar vesicles by a rapid extrusion procedure. Characterization of size distribution, trapped volume and ability to maintain a membrane potential. *Biochim. Biophys. Acta*. 812:55–65.

Hotani, H., and H. Miyamoto. 1990. Dynamic features of microtubules as visualized by dark field microscopy. *Adv. Biophys*. 26:135–156.

Hotani, H., F. Nomura, and Y. Suzuki. 1999. Giant liposomes: from membrane dynamics to cell morphogenesis. *Curr. Opin. Colloid Interface Sci*. 4:358–368.

Isambert, H., P. Venier, A. Maggs, A. Fattoum, R. Kassab, D. Pantaloni, and M. Carlier. 1995. Flexibility of actin filaments derived from thermal fluctuations. *J. Biol. Chem*. 270:11437–11444.

Israelachvili, J. 1992. Intermolecular and Surface Forces. Academic Press, London.

Jass, J., T. Tjärnhage, and G. Puu. 2000. From liposomes to supported, planar bilayer structures on hydrophilic and hydrophobic surfaces: an atomic force microscopy study. *Biophys. J*. 79:3153–3163.

Kabsch, W., G. Mannherz, D. Suck, F. Pai, and C. Holmes. 1990. Atomic structure of the actin:Dnase I complex. *Nature*. 347:37–44.

Korgel, B. A., J. H. van Zanten, and H. G. Monbouquette. 1998. Vesicle size distributions measured by flow field-flow fractionation coupled with multiangle light scattering. *Biophys. J*. 74:3264–3272.

Laliberte, A., and C. Gicquaud. 1988. Polymerization of actin by positively charged liposomes. *J. Cell Biol*. 106:1221–1227.

Lodish, H., A. Berk, S. Zipursky, P. Matsudaira, D. Baltimore, and J. Darnell. 1999. W. H. Freeman and Company, New York.

Miyata, H., and H. Hotani. 1992. Morphological changes in liposomes caused by polymerization of encapsulated actin and spontaneous formation of actin bundles. *Proc. Natl. Acad. Sci. USA*. 89:11547–11551.

Miyata, H., S. Nishiyama, K. Akashi, and K. Kinosita, Jr. 1999. Protrusive growth from giant liposomes driven by actin polymerization. *Proc. Natl. Acad. Sci. USA*. 96:2048–2053.

New, R. R. C. 1990. Liposomes. Oxford University Press, Oxford, UK.

Olson, F., C. A. Hunt, F. C. Szoka, W. J. Vail, and D. Papahadjopoulos. 1979. Preparation of liposomes of defined size distribution by extrusion through polycarbonate membranes. *Biochem. Biophys. Acta*. 557:9–23.

Ott, A., M. Magnasco, A. Simon, and A. Libchaber. 1993. Measurement of the persistence length of polymerized actin using fluorescence microscopy. *Phys. Rev. E*. 48:1642–1645.

Puu, G., I. Gustafson, M. Lundström, and J. Jass. 2000. Distribution and stability of membrane proteins in lipid membranes on solid supports. *Biosens. Bioelectron*. 15:31–41.

Renault, A., P.-F. Lenne, C. Zakri, A. Aradian, C. Vénien-Bryan, and F. Amblard. 1999. Surface-induced polymerization of actin. *Biophys. J*. 76:1580–1590.

Rioux, L., and C. Gicquaud. 1985. Actin paracrystalline sheets formed at the surface of positively charged liposomes. *J. Ultra. Res*. 92:42–49.

Reviakine, I., and A. Brisson. 2000. Formation of supported phospholipid bilayers from unilamellar vesicles investigated by atomic force microscopy. *Langmuir*. 16:1806–1815.

Shao, Z., and J. Yang. 1995. Progress in high resolution atomic force microscopy in biology. *Quar. Rev. Biophys*. 28:195–251.

Sheterline, P., J. Clayton, and J. C. Sparrow. 1995. Actins, 3rd ed. Academic Press, San Diego, CA.

Stauch, O., T. Uhlmann, M. Fröhlich, R. Thomann, M. El-Badry, Y.-K. Kim, and R. Schubert. 2002. Mimicking a cytoskeleton by coupling poly(*n*-isoproplyacrylamide) to the inner leaflet of liposomal membranes: effects of polymerization on vesicle shape and polymer architecture. *Biomacromolecules*. 3:324–332.

Teschke, O. 2002. Liposome structure imagining by atomic force microscopy: verification of improved liposome stability during adsorption of multiple aggregated vesicles. *Langmuir*. 18:6513–6520.

Thomson, N. H., I. Collin, M. C. Davies, K. Palin, D. Parkins, C. J. Roberts, S. J. B. Tendler, and P. M. Williams. 2000. Atomic force microscopy of cationic liposomes. *Langmuir*. 16:4813–4818.

van Zanten, J. H. 1996. Characterization of vesicles and vesicular dispersions via scattering techniques. *In* Vesicles. M. Rosoff, editor. Marcel Dekker, New York. 239–294.

Zimm, B. 1948a. The scattering of light and the radial distribution function of high polymer solutions. *J. Chem. Phys*. 16:1093–1099.

Zimm, B. 1948b. Apparatus and methods for measurement and interpretation of the angular variation of light scattered; preliminary results on polystyrene solutions. *J. Chem. Phys*. 16:1099–1116.